SOFT ROBOTICS
Volume 2, Number 00, 2014

DOI: 10.1089/soro.2014.0016

SoRo
Soft Robotics

ORIGINAL ARTICLE

Finite Element Analysis and Design Optimization of a Pneumatically Actuating Silicone Module for Robotic Surgery Applications

Yahya Elsayed,[1] Augusto Vincensi,[1] Constantina Lekakou,[1] Tao Geng,[2] C. M. Saaj,[2] Tommaso Ranzani,[3] Matteo Cianchetti,[3] and Arianna Menciassi[3]

Abstract

The design of a pneumatically actuated silicone module, resembling soft tissue, with three pneumatic chambers is considered and optimized in this study with the aim of using it in a soft robot arm for robotic surgery applications. Three types of silicone materials, Ecoflex 0030 and 0050 and Dragonskin 0030, have been investigated, and a constitutive model has been derived for each of them. Design optimization of the silicone module was based on finite element analysis (FEA) that was validated against experimental data of one-degree bending under one-channel actuation. This was followed by FEA parametric studies for module design optimization to minimize the ballooning effect in one-degree bending as well as reduce the actuation pressure. Modules made from Ecoflex 0030 and Ecoflex 0050 exhibited the same bending shape in FEA, but about three times higher actuation pressure was required for the harder Ecoflex 0050. Design parameters under investigation in the parametric FEA studies included the shape of the pneumatic channel cross section, the ratio of channel length to module length, the distance of channel from the module wall, and the ratio of channel to module cross-sectional area. After FEA design optimization yielded least ballooning for pneumatic chambers of semicircular cross section, an internal dragonskin structure was added internally below the module surface to enable and guide the bending under one-channel pneumatic actuation and further contain the ballooning effect: the benefits of this design were successfully verified under both FEA and experimental analysis.

Introduction

Soft robotics is a new field of robotic engineering[1,2] that furthers the design of flexible robots consisting of an actuating chain of multiple stiff nodes.[3] Soft robots have the potential to be used in surgical applications,[2,4,5] as the fluidlike flexibility and soft materials of these robots offer them the advantage of being able to navigate through narrow passages between organs with minimum harm to the organ soft tissue, covering outer membrane and vascular blood supply. Elastomer-based robotics have shown great promise in developing robots that mimic the muscular hydrostatic systems found in nature[6,7] such as the octopus tentacles,[8,9] caterpillars,[10] jelly fish and asteroids,[11] and elephant trunk.[12,13]

Elastomers are of particular interest in the field of laparoscopic surgery, as they require low actuation stress or pressure for their deformation, are reliable and low-cost materials, and hence can be used in disposable surgical manipulators[14] eliminating the need of maintenance and sterilization of current laparoscopic tools. Furthermore, the use of silicone in the manufacture of implants already used *in vivo* in medicine makes silicone a good candidate for the manufacture of soft medical robot arms, as it will reduce the number of required biocompatibility pretests *in vivo*. Although several elementary designs of soft robotics actuators have been proposed, such as the McKibben's actuator[15] and the triangular configuration of three or a configuration of more such parallel slimline actuators,[16–18] the feasibility of such designs in the robotic field has been studied traditionally in terms of pure geometrical relationships[16] and kinematic algorithms[18,19] with linear dynamics,[20] without taking into account[16] fluid compressibility, which has significant consequences in pneumatic

Departments of [1]Mechanical Engineering Sciences and [2]Electronic Engineering, University of Surrey, Guildford, United Kingdom.
[3]The BioRobotics Institute, Scuola Superiore Sant'Anna, Pontedera, Italy.

actuators, nonlinear elastomer mechanics, and chamber cross-sectional shape.

The present study also considers a triangular configuration of parallel pneumatic actuators and applies a comprehensive computer-aided design (CAD) and finite element analysis (FEA) to fully consider the shape of the actuating channel and configuration cross sections, compressibility effects of the pneumatic cavity, and elastomer mechanics of three different grades of silicone considered in this study. Furthermore, by processing the results of computer simulations into dimensionless groups and normalizing all lengths with respect to the corresponding nominal length in the same direction, the graphs of the design and optimization studies in this article are generalized and may be extended beyond the scale and application of the particular problem targeted in our case.

The first designs of pneumatic silicone actuators included the bending mode and were intended as a flexible micro-actuator for applications of a bigger soft-bodied robot.[11,21] Such designs were extended as actuator components in soft-robot applications, such as fingers in a robot hand[22] and as module in a robot arm of multiple soft modules for robotic surgery.[23,24] Pneumatic actuator designs have included bending with one degree of freedom comprising one bellow-shaped silicone side over a flat side[25] or pneumatic networks over a flat side,[26] two degrees of freedom comprising two opposite-located pneumatic chambers of different shapes,[11] or three degrees of freedom comprising three pneumatic chambers separated by straight walls.[21,23,24,27] A major concern for a pneumatically actuating robot arm to be used internally in medical diagnosis and surgery is the ''ballooning'' effect under pneumatic actuation[28] where excessive ''ballooning'' and abrupt change of the contour shape may exert excessive local pressure on tissue organs or cause bursting of the silicone module. Furthermore, the ballooning effect in a soft robot essentially wastes energy on radial expansion where the energy needs to be exercised on longitudinal expansion. A crimped braided sleeve devised to constrain excessive radial expansion may cause scratching, organ erythema, or hematoma when under pressure onto adjacent tissue organs as we found in preliminary medical tests[5] for some types of such sleeves.

Hence, the aim of this study was to focus on a pneumatically actuating module made entirely from silicone materials, to investigate different designs of pneumatic chambers for this actuating module in bending with three degrees of freedom, and to optimize the overall soft actuator design using the finite element method to reduce the ballooning effect, while the required actuation pressure level and resulting stress distribution were also taken into account. Figure 1 presents the investigated pneumatic chamber designs of a cylindrical module including (a) three chambers of circular cross section; (b) three chambers of semicircular cross section with the smaller flat surface by the core to facilitate bending of each chamber in the desired direction; (c) three chambers of circular sector cross section, that is, separated by flat walls; and (d) three chambers of circular ring-sector cross section. A hyperelastic constitutive model was fitted from the experimental mechanical test data for alternative elastomeric silicone materials: Ecoflex-0030 and Ecoflex-0050 used for the soft actuating module and Dragonskin 0030 used to fabricate an accordionlike structure near the surface of the actuating module to further control the ballooning effect in an innovative design proposed in this study. The FEA was validated by comparing predictions with experimental data, and it was then used for module design development and optimization.

Materials and Experimental Methods

Two grades of platinum-catalyzed curing silicone were used to fabricate the actuator module, Ecoflex 0030 and 0050, their code numbers referring to the material's shore hardness. These silicone materials come in two parts that were mixed together at a 50:50 mass ratio. The mixture was subjected to vacuum for a period of 15 min to de-air and was then slowly poured in the appropriate mold. The silicone was allowed to cure in the oven at 120°C for 1 h. Dragonskin 0030 (also a two-part mixture at a 50:50 mass ratio) was used in a final module design with an accordionlike structure at the periphery of the cylindrical module using another appropriate mold while the module was placed into a third cylindrical mold of larger diameter into which Ecoflex 0030 was poured to fill the gaps between the harder accordion folds.

Uniaxial tensile testing was conducted on 30 mm × 6 mm × 3 mm strips of all three silicone grades above, using an Instron tensile testing machine with a 100 N load cell, at 300 mm/min

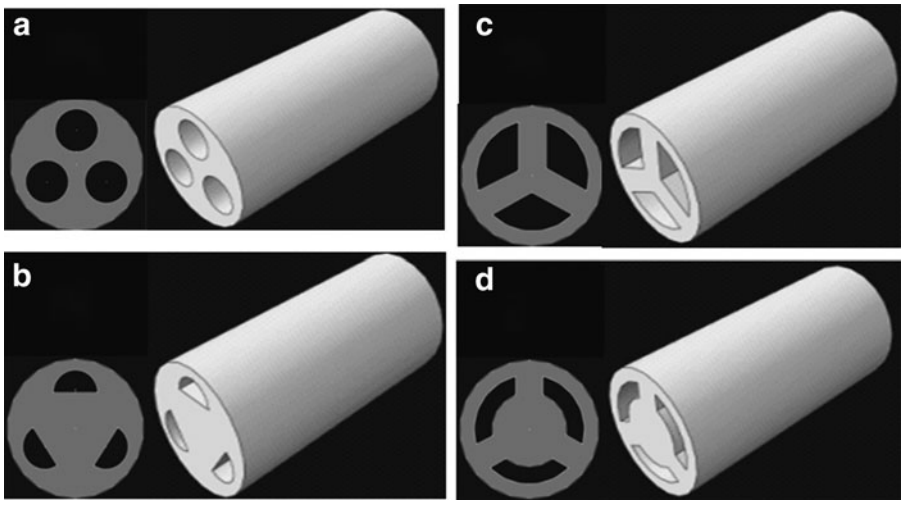

FIG. 1. Investigated pneumatic chamber designs for the pneumatic actuator module for a soft-arm medical surgical robot; module diameter is 25 mm; cross-section of the three pneumatic chambers: **(a)** circular cross-section; **(b)** semicircular cross-section; **(c)** circular sector cross-section; **(d)** ring sector cross-section.

crosshead speed, where the top and bottom 5 mm parts of the samples were clamped using pneumatic force grips.

Figure 2 presents the actuation and tip position track system for a silicone module with three pneumatic chambers. An air compressor was used for the pneumatic actuation, which was driven by a computer-controlled system of three solenoid valves, one for each pneumatic chamber. Actuation pressure for each chamber was varied in the range of 0.1–0.3 bar. A trakStar magnetic sensor was placed at the center of the module's tip in order to sense the real-time 3D position and orientation of the module's tip during actuation. In the experiments of this study, only one chamber was actuated for the module to perform 2D bending on a vertical plane. A video camera was used to record the module deformation during bending for different actuation pressures.

Results

Constitutive model fitting for the tested silicone grades

Reduced N-order polynomial hyperelastic material models represented by Equation 1 were investigated in the fitting of the tensile test data for the silicone materials,[29] where the material was considered incompressible and the strain energy potential U is independent from the second invariant:

$$U = \sum_{i=1}^{N} C_{10}(\bar{I}_1 - 3)^i \tag{1}$$

$\bar{I}_1$ is the first deviatoric strain invariant and C_{ij} is a material-specific parameter. The Ogden model ($N=3$) was also investigated, represented by Equation 2 for the strain energy potential U as a function of deviatoric principal stretches λ_i and is represented by the following relation for incompressible materials:

$$U = \sum_{i=1}^{N} \frac{2\mu_i}{\alpha_i^2}(\lambda_1^{\alpha_i} + \lambda_2^{\alpha_i} + \lambda_3^{\alpha_i} - 3) \tag{2}$$

where μ_i and α_i are empirical parameters.

These models were tried in fitting the experimental data of the mechanical tests for the tested grades of silicone in the strain range of 0–300% (or maximum strain for Dragonskin 0030), where the least square curve fit was used to determine the coefficients for the strain energy equation. Figure 3 presents the tensile test experimental data and best constitutive model fits for the three silicone grades. The third-order reduced polynomial model (Yeoh model, Eq. 1) proved to be the best constitutive model for Ecoflex 0030 with parameter values $N=3$, $C_{10}=5072\,\mathrm{J\cdot m^{-3}}$, $C_{20}=-331\,\mathrm{J\cdot m^{-3}}$, and $C_{30}=-15\,\mathrm{J\cdot m^{-3}}$. The Ogden model (Eq. 2) proved to be the best constitutive model for Ecoflex 0050 with parameter values $N=3$, $\alpha_1=1.55$, $\mu_1=107.9\times10^3\ \mathrm{J\cdot m^{-3}}$, $\alpha_2=7.86$, $\mu_2=21.47\,\mathrm{J\cdot m^{-3}}$, $\alpha_3=-1.91$, and $\mu_3=-87.1\times10^3\ \mathrm{J\cdot m^{-3}}$. The second-order reduced polynomial model (Eq. 1) proved to be the best constitutive model for Dragonskin 0030 with parameter values $N=2$, $C_{10}=1190\,\mathrm{J\cdot m^{-3}}$, and $C_{20}=23{,}028\,\mathrm{J\cdot m^{-3}}$.

Module actuation: experimental studies and FEA validation for different silicone materials

First of all, a series of FEA simulations were carried out for the bending of an Ecoflex 0030 module with three circular cross-sectional chambers, under the pneumatic actuation of one chamber only under different pressures. The bending angle of the tip of the module was determined from the results of the deformed shapes at all pressures and was compared with the experimental data as measured by the tip-tracking magnetic sensor for the corresponding actuation experiments. This comparison is shown in Figure 4a. It seems that there is a transition pressure in the range of 0.06–0.08 bar between the region of relatively small bending angles (0–20°) and the region of high bending angles (>150°), which has been captured accurately by the FEA. On the other hand, the FEA-predicted bending angles at the tip of the actuator lag behind the experimental data. Figure 4b presents the comparison between experiment and FEA predictions of the deformed shape of the Ecoflex 0030 module driven by one

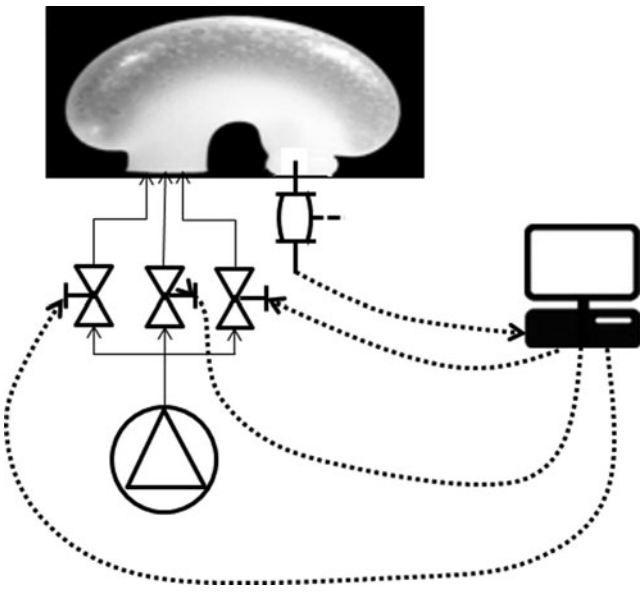

FIG. 2. Diagram of actuation and tip position track system for a silicone module with three pneumatic chambers.

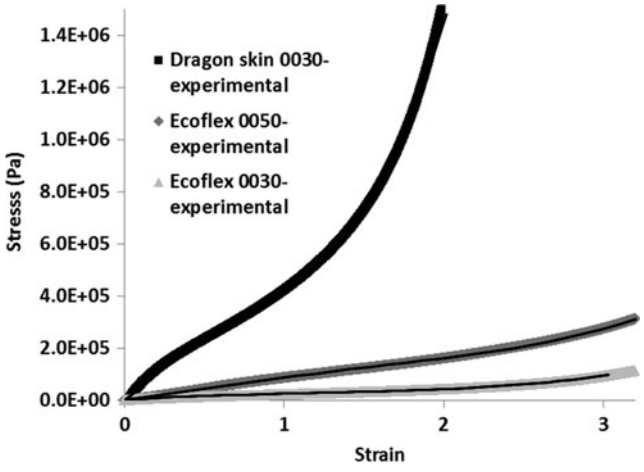

FIG. 3. Best constitutive model stress–strain lines against the corresponding experimental data: Yeoh constitutive model for Ecoflex 0030 and Ogden constitutive model ($N=3$) for Ecoflex 0050 and second-order reduced polynomial for Dragonskin 0030.

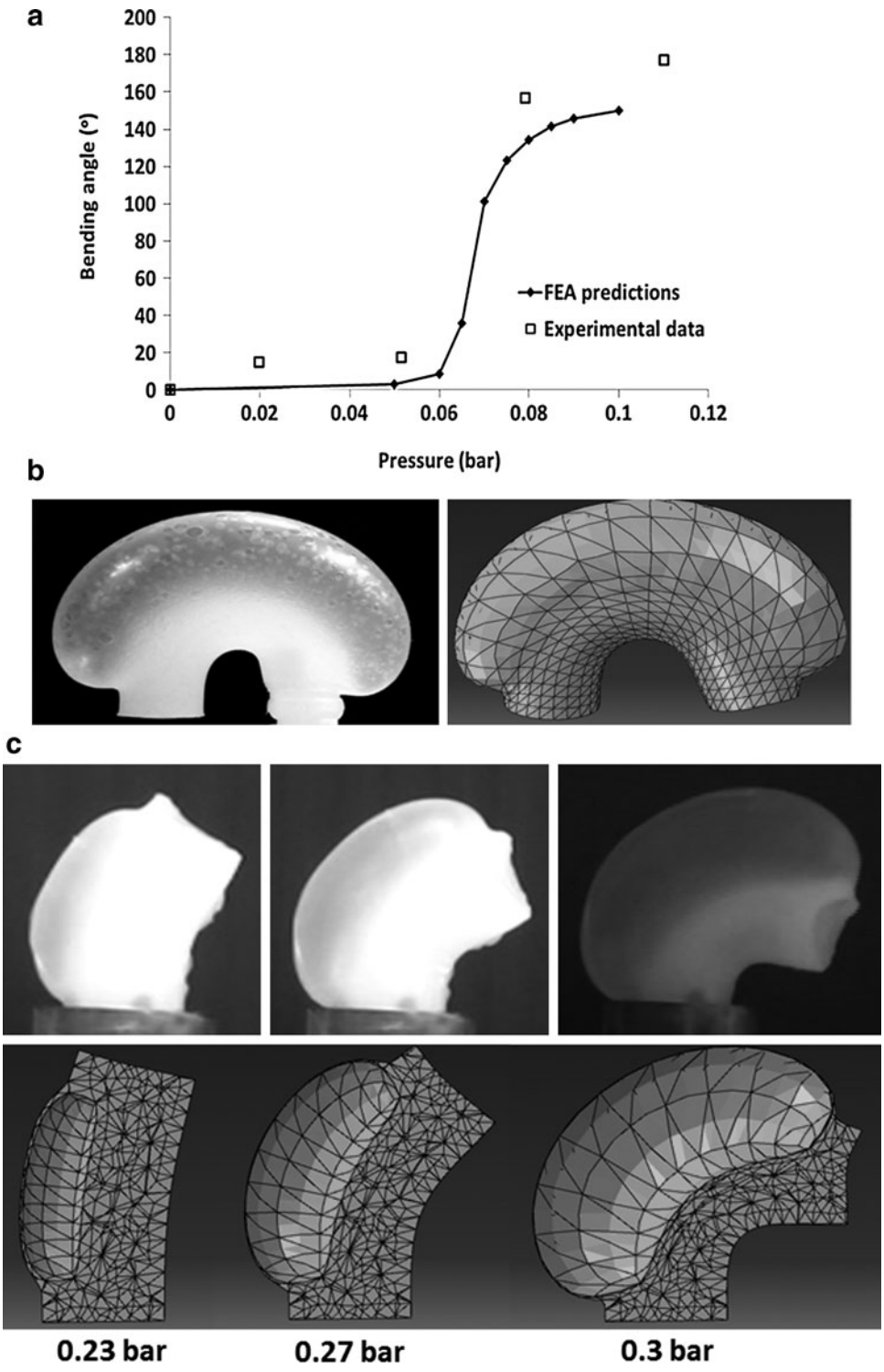

FIG. 4. Experiment versus finite element analysis (FEA) predictions of module bending under one-chamber actuation **(a)** FEA predictions and experimental data from the tip-tracking magnetic sensor of the bending angle at the tip of an Ecoflex 0030 module (three circular cross-sectional chambers, length = 8 mm). **(b)** Ecoflex 0030 module under one-chamber actuation at 0.1 bar. **(c)** Ecoflex 0050 module (three semicircular pneumatic chambers) under one-chamber actuation.

pneumatic chamber at 0.1 bar: using image analysis tools, the maximum radial width of the expanded silicone module (experimental) was measured to be 41.2 mm against the original 25 mm, whereas the FEA-predicted radial width was 40.7 mm at the same actuating pressure.

Figure 4c presents a comparison between FEA predictions and experiment for the case of an Ecoflex 0050 module actuating in bending, driven by different pressures. In general, the radial expansion of the silicone module under pressure can be modeled accurately by the FEA model, although the predictions of bending angle lag behind the experiment, similarly to Ecoflex 0030. It was noticed that the actuation process during the experiment was not at a constant rate under each applied pressure, which, in combination with the FEA bending angle predictions being a little lower than the corresponding experimental values, may indicate the need for a viscoelastic constitutive model. Experimental studies and dynamic modeling of McKibben-type of actuators have also demonstrated rate-dependent effects modeled by damping terms in the dynamic model.[30]

Figure 5 illustrates that modules made from different grades of silicone of different hardness achieve similar deformed shape for the same bending angle, but of course the softer Ecoflex 0030 module requires about 1/3 of the pressure driving the Ecoflex 0050 module to realize the same extent of bending. The generated stress distribution is of particular interest for two reasons: (a) to avoid bursting of the created balloon in the pneumatic chamber under pressure, and (b) to stiffen the actuated module so that the robot arm is stable in its deformed shape for the surgeon to be able to perform the required tasks of gripping, prodding, and cutting using separate slimmer arms or fingers that will protrude out of the tip of the proposed silicone module arm. Figure 5 demonstrates that the outer surface of the balloon in the Ecoflex 0050 module reaches a von Mises stress of 5 MPa for driving pressures greater than 0.26 bar, homogeneously distributed across the length of the balloon. Higher driving pressures above 0.35 bar resulted in bursting the balloon in the Ecoflex 0050 module. The Ecoflex 0030 module reaches a much lower maximum von Mises stress in the range of 0.5–0.9 MPa at a tested driving pressure of 0.1 bar. The maximum force that can be exerted by the tip of the module was also estimated for both types of silicone module for a contact surface area of 2.5×10^{-5} m^2 at the tip of the module to reach 2.4 and 4.6 N for the Ecoflex 0030 and 0050 modules bent under pressure 0.1 and 0.3 bar, respectively.

FEA parametric studies for design optimization of the silicone module

FEA parametric studies of the Ecoflex 0030 silicone module were conducted for module design optimization based on the CAD models of Figure 1 under pressure actuation of one pneumatic chamber to realize one-degree bending of module.

Starting with the semicircular cross-sectional chamber design (Fig. 1b), which in fact proved the chamber design causing the least ballooning as will be seen in later parametric studies, the effect of the chamber-module wall distance was studied normalized by the total module diameter. The standard geometry was a module of 25 mm diameter and 65 mm length, 55 mm chamber length, 3.7 mm chamber radius, and 1.5 mm distance between the chamber wall and the outer module surface. Figure 6a presents the effect of the distance between the pneumatically pressurized chamber and the module's outer surface on the pressure required to reach 90° bending and the balloon side-projected area as in Figures 4 and 5. As this distance decreases, the pressure required to bend the module to 90° also decreases in a linear manner while the radial expansion and associated balloon area are almost constant. Consequently, a ratio of chamber wall–module wall distance/module diameter of 0.04 seems to be the optimum in Figure 6a, translating to 1 mm chamber wall–module wall distance for a 25-mm-diameter module. However, given the residual deformation and balloon surface thinning of repetitively actuated experimental modules leading to early balloon bursting, 1.5 mm chamber wall–module wall distance was used, translated into a ratio of this distance to module diameter of 0.06, which still corresponds to a relatively low required one-chamber actuation pressure of 0.08 bar as seen in Figure 6a.

The next step was to change the chamber length/module length ratio in the range of 0.6–0.95. Figure 6b shows that the pressure required for 90° module bending decreases linearly as the ratio of chamber length/module length is increased. This is accompanied by a reduction of the radial module

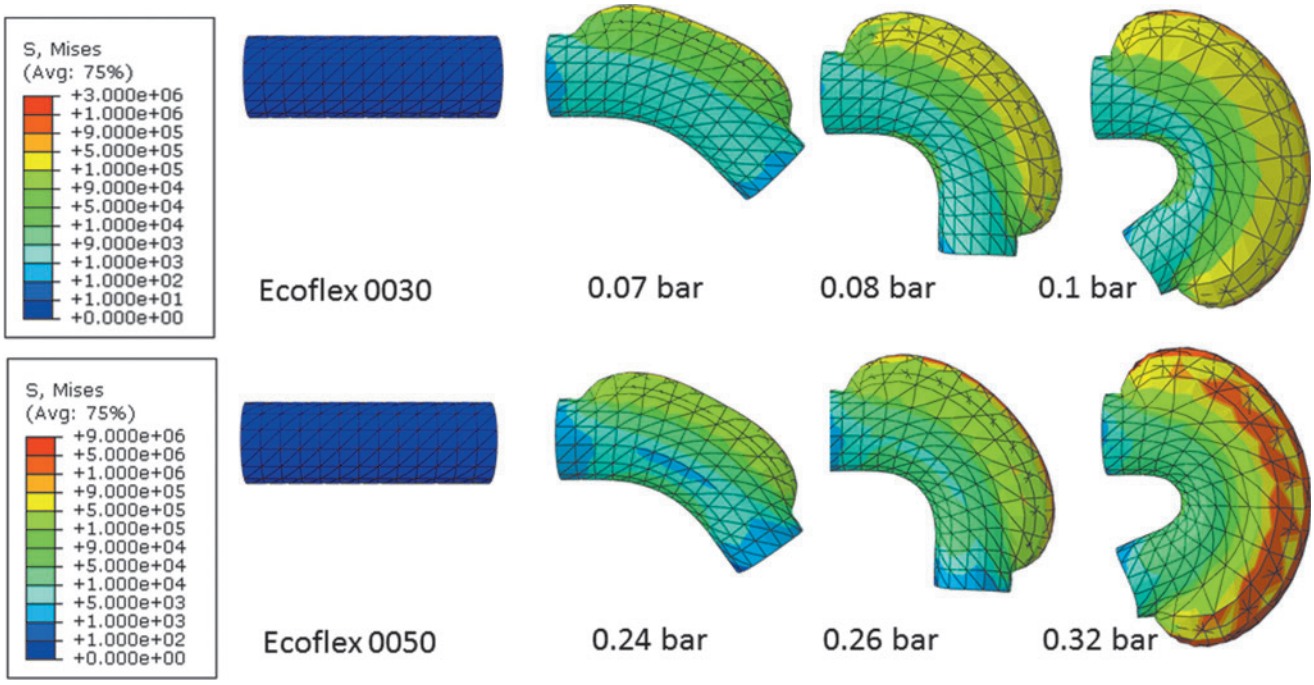

FIG. 5. FEA simulations of a module (with three semicircular pneumatic chambers, length = 8 mm) actuated in one degree of freedom bending mode: comparison between Ecoflex 0030 and Ecoflex 0050 modules at different inputted actuating pressures to achieve the same bending angles in both types of modules. Color images available online at www.liebertpub.com/soro

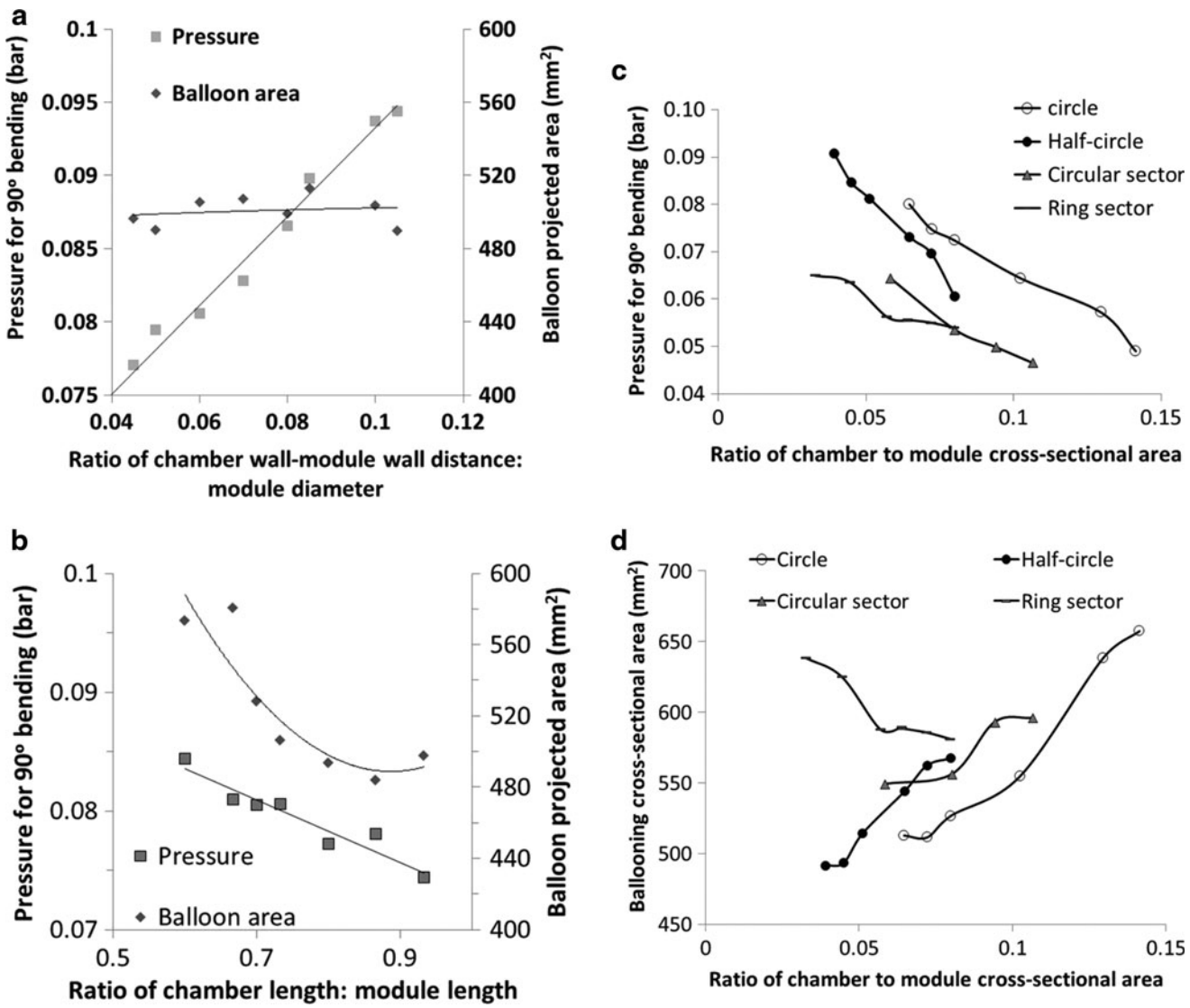

FIG. 6. Results of FEA parametric studies for one-degree actuation of Ecoflex 0030 module: **(a)** effect of the ratio of chamber wall–module wall distance/module diameter on the pressure required for 90° bending and associated balloon-projected area of module with three semicircular chambers; **(b)** effect of the ratio of chamber length/module length on the pressure required for 90° bending and associated balloon-projected area of module with three semicircular chambers; **(c)** effect of the ratio of chamber/module cross-sectional area on the pressure required for 90° bending; **(d)** effect of the ratio of chamber/module cross-sectional area on associated balloon-projected area.

expansion for chamber length/module length ratios between 0.6 and 0.8; further increase of this ratio above 0.8 seems to have little effect on the balloon area. From these findings, it can be concluded that the actuating chamber's length should not be less than 80% of the module's length for the minimum radial expansion, with reduced actuation pressure required to achieve the desired bending. A 55/65 = 0.85 chamber length/module length has been used for the standard 65 mm module, allowing for 5 mm length at the module ends to be able to secure the module easily in a holder during the tests.

The final stage was to consider all four chamber designs proposed in Figure 1 in FEA parametric studies where the cross-sectional area of the chamber was varied with respect to the module cross-sectional area for each type of chamber cross-sectional area design. Figure 6c and d present the results of these studies with the effects on the pressure required to achieve 90° bending of module under one-chamber actuation (Fig. 6c) and the resulted balloon-projected area (Fig. 6d). Figure 6c demonstrates that for all chamber designs the ratio of chamber cross-sectional area/module cross-sectional area has an inverse linear relationship (approximately) with the pressure required to realize 90° module bending under one-chamber actuation. On the other hand, Figure 6d shows a trend for circular, semicircular, and circle-sector chamber cross sections to demonstrate increased radial expansion (increased balloon effect) with increasing the ratio of chamber-to-module cross section.

This increase of the ballooning effect in these three designs is due to the increased surface area of the chamber wall near the outer surface of the module in these types of chambers as the chamber cross-sectional area is increased, offering a larger proportion of thin chamber wall for expansion under

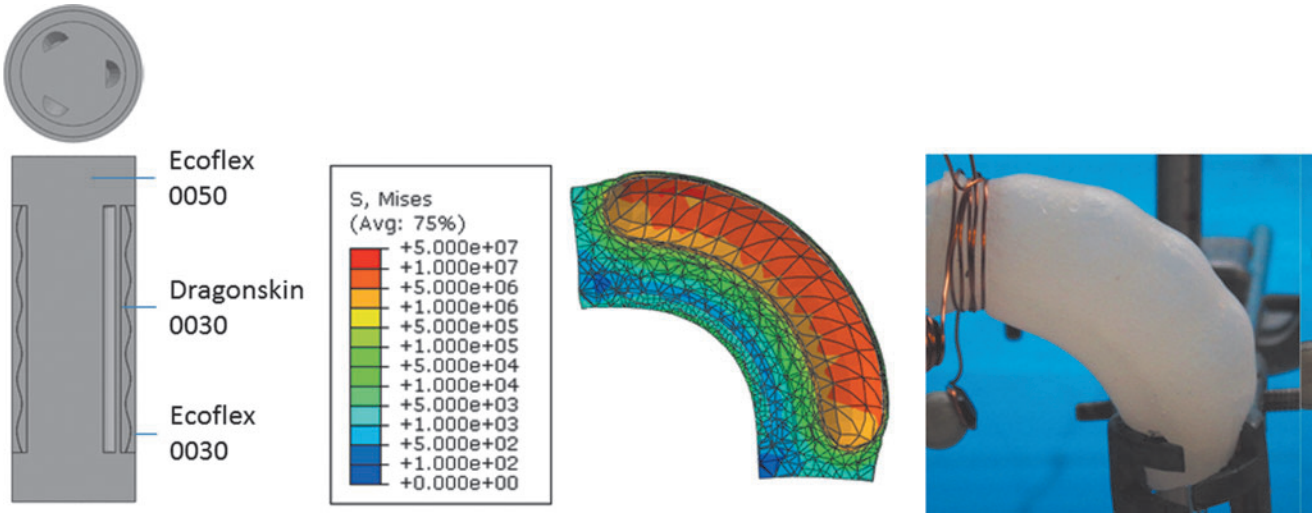

FIG. 7. Module with Dragonskin 0030 accordion structure: module design, FEA analysis, and experimental study of one-chamber actuation under 0.8 bar. Color images available online at www.liebertpub.com/soro

pressure. This, however, is not the case for the ring-sector chamber cross-sectional geometry, as an increase in the chamber's cross-sectional area results in a decrease of the resulted balloon-projected area up to a lower plateau. The reason for this may be attributed to the two almost parallel circumferential sides of the ring-sector cross-sectional geometry of the pneumatic chambers that does not create any effect of increased outer circumferential chamber area when the chamber cross-sectional area is increased.

Figure 6c shows that the optimum design in terms of the least pneumatic actuation pressure required to achieve a 90° module bend with the smallest proportion of chamber area is that with the ring-sector chamber cross section where, for a small chamber/module cross-sectional area ratio of 0.032, this bending is achieved under 0.065 bar one-chamber actuation. Smaller proportion of chamber cross section in the module cross section means that the core of the module can be used for other instruments in the medical robot arm, for example.

The advantage of the ring-sector-shaped chamber cross-sectional design in terms of required actuation pressure is hindered by the disadvantage this chamber design has in terms of radial expansion, where, as is shown in Figure 6d, the ring-sector chamber cross-sectional design is associated with the largest extent of ballooning for all examined chamber: module cross-sectional ratios when compared to all the other chamber designs. The smallest balloon projection area is achieved when using the semicircular chamber cross-sectional design with a chamber/module cross-sectional area ratio of 0.04, which corresponds to a required pressure of 0.08 bar for 90° bend under one-chamber actuation. In general, the pressures used to actuate the module are quite low and within the ranges of medical standards when compared to standard techniques such as for tourniquets in orthopedic surgery, which use pressures around 0.4 bar; hence, the effect on the actuation pressure within the range of these parametric studies (up to 0.09 bar) is given the lowest priority in the optimization process. The highest priority is set to minimize ballooning of the module while maintaining the required extent of bending under one-chamber actuation. Using this criterion, the semicircular chamber cross-sectional geometry has been selected with a chamber/module cross-sectional area ratio between 0.04 and 0.065 (with a higher ratio included to facilitate manufacturing).

Discussion and Conclusion: Final Composite Module Design, FEA Simulation, and Experimental Study

With the aim to further reduce the ballooning effect while the module still maintains its good bending capability upon actuation, a corrugated accordionlike outer layer from Dragonskin 0030 was added to the optimized module from Ecoflex 0050, while soft Ecoflex 0030 was used to fill the gaps between the corrugations for the module to present a smooth outer surface if in contact with the internal organs in robotic surgery. Figure 7 presents the innovative module design used for an initial FEA simulation and also the FEA simulation results in terms of bending by 90° and the contours of the von Mises stress in a cross section displaying clearly the balloon cross section with a very small increase of the module diameter by only 16%. The experimental study of the same module in Figure 7 shows larger ballooning with an increase of the module diameter by 26%. However, this is still less than the ballooning of the standard optimized module from Ecoflex 0050 without the dragonskin structure that experiences a larger ballooning effect with an increase of the module diameter by 60%.

Acknowledgments

We would like to gratefully acknowledge support of this work by the European Community–funded research project STIFF-FLOP (FP7-ICT-287728).

Author Disclosure Statement

No conflicts of interest exist, and no commercial, equipment, or material supplier funding was received.

References

1. Ilievski F, Mazzeo AD, Shepherd RF, Chen X, Whitesides GM. Soft robotics for chemists. Angew Chem Int Ed 2011; 50:1890–1895.

2. Ding J, Goldman RE, Xu K, Allen PK, Fowler DL, Simaan N. Design and coordination kinematics of an insertable robotic effectors platform for single-port access surgery. IEEE/ASME Trans Mechatron 2013;18:1612–1624.
3. Grzesiak A, Becker R, Verl A. The bionic handling assistant—a success story of additive manufacturing. Assembly Automation 2011;31:329–333.
4. Neuzil P, Cerny S, Kralovec S, Svanidze O, Bohuslavek J, Plasil P, Jehlicka P, Holy F, Petru J, Kuenzler R, Sediva L. Single-site access robot-assisted epicardial mapping with a snake robot: preparation and first clinical experience. J Robot Surg 2013;7:103–111.
5. Elsayed Y, Lekakou C, Ranzani T, Cianchetti M, Morino M, Arezzo A, Menciassi A, Geng T, Saaj CM. Crimped braided sleeves for soft, actuating arm in robotic abdominal surgery. Minim Invasive Ther Allied Technol 2014; (in press).
6. Trivedi D, Rahn CD, Kier WM, Walker ID. Soft robotics: biological inspiration, state of the art, and future research. Appl Bionics Biomech 2008;5:99–117.
7. Kim S, Laschi C, Trimmer B. Soft robotics: a bioinspired evolution in robotics. Trends Biotechnol 2013;31:287–294.
8. Walker ID, Dawson D, Flash T, Grasso F, Hanlon R, Hochner B, Kier WM, Pagano C, Rahn CD, Zhang Q. Continuum robot arms inspired by cephalopods. Proceedings of the SPIE Conference on Unmanned Ground Vehicle Technology VII, Orlando, FL, USA, 2005, pp. 303–314.
9. Laschi C, Cianchetti M, Mazzolai B, Margheri L, Follador M, Dario P. Soft robot arm inspired by the octopus. Adv Robot 2012;26:709–727.
10. Lin H-T, Leisk GG, Trimmer B. GoQBot: a caterpillar-inspired soft-bodied rolling robot. Bioinsp Biomimet 2011; 6:026007.
11. Suzumori K, Endo S, Kanda T, Kato N, Suzuki H. A Bending pneumatic rubber actuator realizing soft-bodied manta swimming robot. Proceedings of the 2007 IEEE International Conference on Robotics and Automation, Rome, Italy, 2007, pp. 4975–4980.
12. Wilson JF, Li D, Chen Z, George RT. Flexible robot manipulators and grippers: relatives of elephant trunks and squid tentacles. In: Robots and Biological Systems: Toward a New Bionics? Dario P, *et al*. (eds.). Berlin: Springer–Verlag, 1993, pp. 474–479.
13. Cieslak R, Morecki A. Elephant trunk type elastic manipulator—a tool for bulk and liquid type materials transportation. Robotica 1999;17:11–16.
14. Cosentino F, Tumino E, Rubis Passoni G, Rigante A, Barbera R, Tauro A, Cosentino FE. Robotic colonoscopy. In: Colonoscopy. Miskovitz P (ed.), InTech, 2011. Available at www.intechopen.com/books/colonoscopy/roboticcolonoscopy
15. Klute G, Czerniecki J, Hannaford B. Mckibben artificial muscles: pneumatic actuators with biomechanical intelligence. Proceedings of the IEEE/ASME International Conference on Advanced Intelligent Mechatronics, Atlanta, GA, USA, 1999, pp. 221–226.
16. Bishop-Moser J, Krishnan G, Kim C, Kota S. Design of soft robotic actuators using fluid-filled fiber-reinforced elastomeric enclosures in parallel combinations. Proceedings of the IEEE/RSJ International Conference on Intelligent Robot Systems (IROS), Algarve, Portugal, 2012, pp. 4262–4269.
17. McMahan W, Pritts M, Chitrakaran V, Dienno D, Grissom M, Jones B, Csencsits M, Rahn CD, Dawson D, Walker LD. Field trials and testing of ''OCTARM'' continuum robots. Proceedings of the IEEE International Conference on Robotics and Automation, Orlando, FL, USA, 2006, pp. 2336–2341.
18. Pritts MB, Rahn CD. Design of an artificial muscle continuum robot. Proceedings of the IEEE International Conference on Robotics and Automation, New Orleans LA, USA, 2004, pp. 4742–4746.
19. Godage IS, Nanayakkara T, Caldwell DG. Locomotion with continuum limbs. Proceedings of the IEEE/RSJ International Conference on Intelligent Robot Systems (IROS), Algarve, Portugal, 2012, pp. 293–298.
20. Lane DM, Davies JBC, Robinson G, O'Brien DJ, Sneddon J, Seaton E, Elfstrom A. The AMADEUS dextrous subsea hand: design, modeling, and sensor processing. IEEE J Oceanic Eng 1999;24:96–111.
21. Suzumori K, Iikura S, Tanaka H. Development of flexible microactuator and its applications to robotic mechanisms. Proceedings of the 1991 IEEE International Conference on Robotics and Automation, Sacramento, CA, USA, 1991, pp. 1622–1627.
22. Suzumori K, Iikura S, Tanaka H. Applying a flexible microactuator to robotic mechanisms. IEEE Control Syst 1992; 12:21–27.
23. Ranzani T, Cianchetti M, Gerponi G, De Falco I, Petroni G, Menciassi A. A modular soft manipulator with variable stiffness. 3rd Joint Workshop on New Technologies for Computer/Robot Assisted Surgery, 2013.
24. Cianchetti M, Ranzani T, Gerponi G, Nanayakkara T, Althoefer K, Dasgupta P, Menciassi A. Soft robotics technologies to address shortcomings in today's minimally invasive surgery: the STIFF-FLOP approach. Soft Robot 2014;1:122–131.
25. Wakimoto S, Suzumori K, Ogura K. Miniature pneumatic curling rubber actuator generating bidirectional motion with one air-supply tube. Adv Robot 2011;25:1311–1330.
26. Martinez RV, Glavan AC, Keplinger C, Oyetibo AI, Whitesides GM. Soft actuators and robots that are resistant to mechanical damage. Adv Funct Mater 2014;24:3003–3010.
27. Chang B, Chew A, Naghshineh N, Menon C. A spatial bending fluidic actuator: fabrication and quasi-static characteristics. Smart Mater Struct 2012;21:045008.1–7.
28. Hoeg HD, Slatkin AB, Burdick JW, Grundfest WS. Biomechanical modeling of the small intestine as required for the design and operation of a robotic endoscope. Proceedings of the 2000 IEEE International Conference on Robotics and Automation, San Francisco, CA, USA, 2000, vol. 2, pp. 1599–1606.
29. Podnos E, Becker E, Klawitter J, Strzepa P. FEA analysis of silicone MCP implant. J Biomech 2006;39:1217–1226.
30. Balasubramanian S, Ward J, Sugar T, He J. Characterization of the dynamic properties of pneumatic muscle actuators. Proceedings of the IEEE International Conference on Rehabilitation Robotics, Noordwijk, Netherlands, 2007, pp. 764–770.

Address correspondence to:
Constantina Lekakou, PhD
Department of Mechanical Engineering Sciences
University of Surrey
Guildford, Surrey
England GU2 7XH
United Kingdom

E-mail: c.lekakou@surrey.ac.uk